Cu(II) and Zn(II) complexes with a poly-functional ligand derived from *o*-vanillin and thiophene. Crystal structure, physicochemical properties, theoretical studies and cytotoxicity assays against human breast cancer cells

María R. Rodríguez [a], Julián Del Plá [a], Lucía M. Balsa [a], Ignacio E. León [a], Oscar E. Piro [b], Gustavo A. Echeverría [b], Javier García-Tojal [c], Reinaldo Pis-Diez [a], Beatriz S. Parajón-Costa [a] and Ana C. González-Baró [a] [*]

[a] CEQUINOR (CONICET-CCT La Plata, UNLP), Bvd. 120 N°1465, B1900AVV La Plata, Argentina.

[b] IFLP (CONICET-CCT La Plata, UNLP), CC 67, B1900AVV, La Plata, Argentina.

[c] Departamento de Química, UBU, Pza. Misael Bañuelos s/n, E-09001 Burgos, España.

Abstract

The interaction of a poly-functional ligand derived of *o*-vanillin and 2-thiophenemethylamine (oVATPNH2) with transition metal ions, Cu(II) and Zn(II) leads to the formation of stable coordination compounds, namely [Cu(oVATPNH2)$_2$] and [Zn(oVATPNH2)$_2$]. Their crystal structures have been determined by X-ray diffraction methods. Two molecules of the deprotonated ligand acting as bidentate build a nearly square planar environment around Cu(II) and a distorted tetrahedral coordination arrangement for Zn(II). The complexes were characterized by spectroscopic techniques, including solid state FTIR, Raman, EPR and diffuse reflectance and solution UV-vis and EPR. Their thermal behavior has been analyzed by means of TGA and DTA. DFT theoretical studies, using computational methods based on DFT, were employed to assist the interpretation and assignment of spectroscopic data. Cytotoxicity assays against two human breast cancer cell lines, namely MCF-7 and MDA-MB-231, revealed an enhancement of effectiveness of the complexes as compared with both the ligand and the free metal ions. The results for the copper compound are promising, as its cytotoxic effect was stronger than the reference metallodrug cisplatin in both cancer cell lines tested.

1. Introduction

Coordination chemistry of biological relevant transition metals is a subject of permanent interest in the search of new metallodrugs. A great number of salicylaldehyde derivatives have been extensively employed as active ligands because of their broad variety of applications in many fields, including the therapeutic activity[1-3]. The inclusion of heterocyclic scaffolds in the molecules has been successfully employed in the development of new drugs having a wide range of pharmacological effects, such as antimicrobial, anthelmintic, anti-inflammatory, analgesic, antipyretic, diuretic, hypoglycemic, anticonvulsant, anti-HIV, cytotoxic and antitumor. [4-6] In particular, poly-functional molecules containing thiophene are of special interest because of the participation of this heterocycle in the improvement of

therapeutic agents.[7] Additionally, the sulfur atom can act as a potential donor in the ligands depending on their conformational properties.

The relevance of transition metal coordination chemistry involving this kind of ligands is based on the structural versatility, syntheses accessibility and wide application in different fields. They are of interest in food and dye industries; in analytical and agro-chemistry and they have shown catalytic, antioxidant, fungicidal, anti-inflammatory and antitumor activities.[8-10] It is expected that complexation leads to an improvement in the activity of the ligand or the metal themselves. It is well known that, among the first row of transition metals, copper and zinc are involved in many essential biological roles and in a wide variety of bioinorganic systems. Furthermore, these metals have been important in the development of metallo-pharmaceuticals with diverse therapeutic activity in an attempt to lower the side effects.

Examples of copper complexes involving ligands derived from heterocycles have shown relevant characteristics and applications.[11-13] The interaction of this kind of ligands with the Zn(II) has led to stable complexes that have been studied in relation with the importance of this metal in biological functions and therapeutic activities.[13-16]

Among the diversity of biological and therapeutic effects of metal complexes, antitumor activity is one of the most relevant.[17] In particular, breast cancer is one of the more frequent causes of premature mortality in female population. One of the most aggressive types is the one known as triple-negative breast cancer. Up to the moment, chemotherapy seems to be the only possible treatment, involving side effects. Then, great efforts are devoted to improve therapeutic agents to optimize the treatment.[18]

The selected ligand in this work (oVATPNH2, HL, see Scheme 1) has been obtained and fully characterized in our laboratory.[19] It is the product of the reaction of o-vanillin (2-hydroxy-3-methoxybenzaldehyde, hereafter oVa) and 2-thiophenemethylamine (TPNH2). It is an example of Schiff base derived from primary amines involving a heterocycle, a group of compounds with interesting properties.[4]
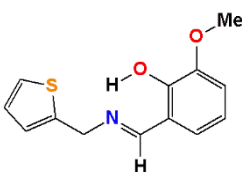
Scheme 1:oVATPNH2, HL ligand (2-methoxy-6-{(E)-[(thiophen-2-ylmethyl)imino]methyl}phenol).

According to the structural properties of oVATPNH2, it could be considered as a candidate for a three dentate ligand with O, N, S donor atoms. Although this is not the more typical coordination feature for ligands containing thiophene, it has been proposed in many complexes involving different metallic centers.[20-23] The chelating ability of this compound is examined by its interaction with Cu(II) and Zn(II) and the resulting complexes are presented in this work.

The complexes have been fully characterized by means of spectroscopic (FTIR, Raman, UV-Vis and EPR) techniques, their thermal behavior has been explored by TGA and DTA and their crystal structures were determined by X-ray diffraction methods. DFT calculations were performed to complement experimental results and to assist in their interpretation. The cytotoxic activity of the complexes was essayed against two tumoral cell lines and compared with the free ligand, metal ions and the reference metallodrug cisplatin, with promising results in breast cancer cell lines. The physicochemical and structural characteristics of the compounds that are analyzed herein can help to explain their behavior in chemical or biological reactions, being a valuable tool in the design of new synthetic systems.

2. Experimental

2.1. Synthesis

The following reactants and solvents were used as provided with no further purification. Absolute ethanol (Soria), methanol and acetonitrile (Carlo Erba), $Cu(CH_3COO)_2·H_2O$ (Merck) and $Zn(CH_3COO)_2·2\ H_2O$ (Mallinckrodt).

The ligand oVATPNH2 (HL) was prepared according with previously reported data.[19]

Elemental analyses were performed in an Exeter CE 440 analyser and melting points were determined in a Bock monoscop "M" instrument.

The complexes were prepared according to the following procedures:

[Cu(oVATPNH2)₂] (CuL₂): This complex was prepared from different copper salts, namely chloride, nitrate and acetate and in different solvents (ethanol, methanol, acetonitrile), but only in the following case it was possible to obtain a crystalline product: over a solution of $Cu(CH_3COO)_2·H_2O$ (0,10 mmol, 0.0199 g) in acetonitrile (8 mL), a solution of the ligand (0,20 mmol, 0492 g) in the same solvent (25mL) was drop wise added under stirring and mild heating conditions. The resulting solution immediately changes its colour from yellow to ochre with forward precipitation of yellowish-green crystals. The system was kept in the same conditions for 30 minutes and the solid was isolated by filtration. (Yield: 65%, 0.0361 g, m.p: 237-238°C) Anal. Found: C, 55.98; H, 4.43; N, 5.12; S, 11.48% Calc. for $C_{26}H_{24}N_2O_4S_2Cu$: C, 56.15; H, 4.35; N, 5.04; S, 11.53 %.

[Zn(oVATPNH2)₂] (CuL₂): A solution prepared from 0,1255g of ligand (0,51mmol) in 25 mL of ethanol, under stirring and heating conditions, was let to achieve reflux temperature. Then, 0.0547g (0,25 mmol) of $Zn(CH_3-COO)_2·2H_2O$ (Mallinckrodt) dissolved in 5 mL of the same solvent were drop wise added. After four hours of reflux, a white solid was isolated by filtration and the remaining solution was kept in the refrigerator (4°C, approximately) during one month. A crystalline yellow solid was obtained, filtered off and dried in a dissector. (Yield: 32%, 0.0446 g, m.p: 203-204°C). Anal. Found: C, 55.87; H, 4.45; N, 4.95, S, 11.54 % Calc. for $C_{26}H_{24}N_2O_4S_2Zn$: C, 55.97; H, 4.34; N, 5.02; S, 11.49 %.

2.2. X-ray diffraction data

The measurements of complexes (**I**) and (**II**) were performed on an Oxford Xcalibur Gemini, Eos CCD diffractometer with graphite-monochromated MoKα (λ=0.71073 Å) radiation. X-ray diffraction intensities were collected (ω scans with ϑ and κ-offsets), integrated and scaled with CrysAlisPro [24] suite of programs. The unit cell parameters were obtained by least-squares refinement (based on the angular settings for all collected reflections with intensities larger than seven times the standard deviation of measurement errors) using CrysAlisPro. Data were corrected empirically for absorption employing the multi-scan method implemented in CrysAlisPro. The structures were solved by direct methods with SHELXS of the SHELX suit of programs [25] and the molecular models refined by full-matrix least-squares procedure on F^2 with SHELXL of the same package. At this stage it was noted a rotational disorder of the five-member thiophene ring which splits into a dominant (74% for the Cu complex and 83% for the Zn one) conformer and a second minor one rotated from the first in 180º around the linking C-C σ-bond. This disorder was modeled in terms of two such rings and refined such that their occupancies summed up to one. The hydrogen atoms were located on stereo-chemical basis and refined with the riding model. The methyl groups were refined as rigid group allowed to rotate around the corresponding $O-CH_3$ bonds such as to maximize the sum of the electron density at the hydrogen calculated positions. The methyl group of both complexes converged to staggered angular conformations.

2.3. Spectroscopy

Infrared spectra of solid samples (KBr pellets) were recorded with a Bruker Equinox 55 instrument in the 4000-400 cm^{-1} region. Raman spectra were measured with a WITEC alpha 300 RA spectrophotometer, using laser excitation wavelength of 532 nm and a 20x objective lens.

Electronic spectra of the compounds and reactants were recorded in solution of dimethyl sulfoxide (DMSO), using 10 mm quartz cells in the spectral range from 190 to 800 nm. Diffuse reflectance spectra (convert in absorbance from Kubelka-Munk function) in the 250 - 800 nm range were recorded using $BaSO_4$ pellet as a reference with an integrating sphere attachment. Both spectra were registered in a Shimadzu UV-2006 spectrophotometer.

X-band EPR spectra were acquired on a polycrystalline samples, room temperature and frozen glassy solutions by using a Bruker EMX spectrometer, equipped with a Bruker ER 036TM NMR-teslameter and an Agilent 53150A microwave frequency counter. Variable temperature experiments were precisely controlled by a Bruker ER 4131VT accessory by using the combined action of a liquid nitrogen evaporator, a heater and the BVT3000 temperature controller. A flat quartz cell was used for room-temperature studies in solution, whereas the solvents mixture was quickly frozen inside the standard quartz tube in the experiments at 120 K. SimFonia program [26] was used to perform the

simulated spectra and graphics were carried out with Kaleidagraph v4.1 [27]. Experimental details are given in figure captions.

NMR samples were prepared under a nitrogen atmosphere by dissolving the suitable amount of the compound in 0.5 mL of pre-dried (Molecular Sieves 4Å) oxygen-free $CD_3)_2SO$ and the spectra were recorded at 298 K. Typically, ^1H NMR spectra were acquired with 32 scans into 32 k data points over a spectral width of 16 ppm. ^1H and ^{13}C chemical shifts were internally referenced to TMS via the residual ^1H signal of CHD_2SOCD_3 (δ = 2.50 ppm) and the ^{13}C signal of $(CD_3)_2SO$ (δ = 39.52 ppm), according to the values reported by Fulmer et al.[28] Heteronuclear 2D NMR spectra such as ^1H-^{13}C HSQC, ^1H-^{13}C HMBC were recorded using standard pulse sequences. The probe temperature (±1 K) was controlled by a standard unit calibrated with methanol as a reference. All NMR data processing was carried out using MestReNova version 10.0.2.

2.4. Computational methods.

The structures of the three complexes were optimized using the Becke's three parameters hybrid density functional [29] with the gradient-corrected correlation functional due to Lee, Yang, and Parr [30] as implemented in of the ORCA program [31]. The Def2-TZVP basis set of triple-zeta quality was used for all the atoms.[32] The experimental structures obtained from X ray diffraction were taken as starting geometries for $Cu(oVATPNH_2)_2$ and $Zn(oVATPNH_2)_2$. Based on spectroscopic results, a square pyramidal geometry was proposed in the case of $VO(oVATPNH_2)_2$. Optimizations were conducted in the gas phase.

To verify whether the optimized geometries are local minima or saddle points on the potential energy surface of the molecules the eigenvalues of the Hessian matrix of the total energy with respect to the nuclear coordinates were calculated. Those eigenvalues were then transformed to harmonic vibrational frequencies, which were further used to aid in the assignment of the experimental vibrational frequencies. No factors were used to scale calculated frequencies.

The electronic spectra of complexes were calculated using the hybrid PBE0 functional [33] as implemented in the ORCA program. The Def2-TZVP basis sets were used for those calculations, too. Solvent effects were included implicitly through the Conductor-like Screening Model (COSMO) [34] as implemented in the ORCA program. The results obtained by these procedures were used to assist in the interpretation and assignments of the spectroscopic data.

2.5. Thermal analysis.

The thermal analysis (TG and DT) of the three complexes and the ligand has been performed using Shimadzu TG-50 and DT-50 units, in a 25° to 800 ºC temperature range at a heating rate of 5 ºC min^{-1} and oxygen flow of 80 mL min^{-1}.

2.6. Biological assays.

2.6.1. Materials

Tissue culture materials were purchased from Corning (Princeton, NJ, USA), Dulbecco's modified Eagle's medium (DMEM) and TrypLE ™ were purchased from Gibco (Gaithersburg, MD, USA), and fetal bovine serum (FBS) was purchased from Internegocios (Argentina). All the cell lines were purchased from ATCC (American Type Culture Collection.

2.6.2. Cell line and growth conditions

MCF-7 (breast) cancer cells were grown in DMEM containing 10 % FBS, 100 U/mL penicillin, and 100 µg/mL streptomycin at 37° C in a 5 % CO_2 atmosphere whilst MDA-MB-231 (triple negative breast) were grown in F12-DMEM. Cells were seeded in a 75-cm^2 flask, and when 70–80 % of confluence was reached, cells were subcultured using 1 mL of TrypLE ™ per 25-cm^2 flask. For experiments, cells were grown in multiwell plates. When cells reached the desired confluence, the monolayers were washed with PBS and were incubated under different conditions according to the experiments.

2.6.3. Cell viability study: 3-(4,5-Dimethylthiazol-2-yl)-2,5-diphenyltetrazolium bromide assay

The 3-(4,5-dimethylthiazol-2-yl)-2,5-diphenyltetrazolium bromide (MTT) assay was performed according to Mosmann [35]. Briefly, cells were seeded in a 96-well dish for 24 h, and treated with different concentrations of compound (1-50 µM) at 37° C for 48 h. Afterward, the medium was changed and the cells were incubated with 0.5 mg/mL MTT under normal culture conditions for 3 h. Cell viability was marked by the conversion of the tetrazolium salt MTT to a colored formazan by mitochondrial dehydrogenases. Color development was measured spectrophotometrically with a microplate reader (model 7530, Cambridge Technology, USA) at 570 nm after cell lysis in DMSO (100 µL per well). Cell viability was plotted as the percentage of the control value.

3. Results and discussion

3.1. Crystal Structures

Crystal data and structure refinement results are summarized in Table 1 and ORTEP [36] drawings of the copper and zinc complexes are shown in Figure 1. The metal ion in both complexes is coordinated to two, symmetry-related, Schiff bases acting as bidentate ligands through the phenoxo oxygen and the imine nitrogen atoms. In the copper complex, the metal ion is sited on a crystallographic inversion centre in a nearly square environment often found in Cu(II) coordination compounds [37-39], with d(Cu-O)=1.887(1) Å, d(Cu-N)=1.997(2) Å and ∠(O-Cu-N)=91,25(6)º. In the zinc compound the metal is sited on a two-fold symmetry axis in an squashed tetrahedral environment, typical for Zn(II) and displayed also in complexes with related ligands d(Zn-O)=1.921(2) Å, d(Zn-N)=1.997(2) Å and ∠(O-Zn-

N)=95.88(7)°.[40-42] Complete lists of geometrical parameters are available as supplementary information (Tables S1-S5).

Because of π-bond delocalization, both the arylmethylidenemethanamine and the thiophene fragments are planar [rms deviation of atoms from the corresponding best least-squares planes less than 0.017 Å]. Planarity in the arylmethylidenemethanamine molecular skeleton is further stabilized by the ligand bite-like coordination to metal.

The conformation and metrics of the single-charged anionic ligand can be compared with the corresponding geometric data reported for the uncharged pure oVATPNH2 ligand. It crystallizes in the monoclinic space group $P2_1/n$ with two un-equivalent but structurally closely related molecules per asymmetric unit (Z=8), one of them showing rotational disorder of the five-member ring. The disorder has been modeled in term of two rings rotated from each other in 180° around the linking C-C σ-bond.[19]

Referring to the better refined, disorder-free molecule in the neutral ligand, some bond structure changes are expected upon deprotonation of OH group followed by formation of the metal-O and metal-N bonds. Main change occurs at the C-O bonds as C-OH formally single bond length of 1.351(4) Å shortens to 1.297(2) Å (twelve times the standard deviation σ) in the copper complex and to 1.307(2) Å (12σ) in the zinc complex (see tables S2a,b).
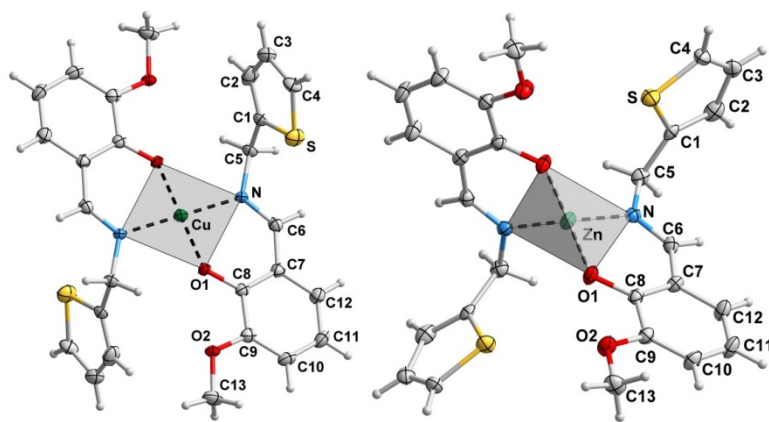
Figure 1: View of [Cu(oVATPNH2)$_2$] (CuL$_2$) (left) and [Zn(oVATPNH2)$_2$] (ZnL$_2$) (right) showing the labeling of the non-H atoms and their displacement ellipsoids at the 30% probability level. The unlabeled atoms are obtained from the labeled ones through a crystallographic inversion center at the copper location and by a 180° rotation around a two-fold axis passing through the zinc ion, respectively. Metal-ligand bonds are indicated by dashed lines. For clarity, in both complexes only it is shown the dominant conformer of the rotationally disordered thiophene group.

**Table 1**. Crystal data and structure refinement for [Cu(oVATPNH2)$_2$] (**I**) and [Zn(oVATPNH2)$_2$] (**II**)

	CuL$_2$	ZnL$_2$
Empirical formula	C$_{26}$H$_{24}$N$_2$O$_4$S$_2$Cu	C$_{26}$H$_{24}$N$_2$O$_4$S$_2$Zn
Formula weight	556.13	557.96
Temperature (K)	293(2)	294(2)
Wavelength (Å)	0.71073	0.71073
Crystal system	Triclinic	Monoclinic
Space group	$P\bar{1}$	C2/c
Unit cell dimensions		
a(Å)	5.2558(3)	22.636(1)
b(Å)	10.5965(5)	5.3423(3)
c(Å)	11.1192(5)	20.8134(8)
α(°)	99.818(4)	90.00
β(°)	91.255(4)	104.814(4)
γ(°)	102.935(4)	90.00
Volume (Å^3)	593.54(5)	2433.3(2)
Z, density (calc., Mg/m^3)	1, 1.556	4, 1.523
Absorpt. coeff. (mm^{-1})	1.133	1.218
F(000)	287	1152
Crystal size (mm^3)	0.307 x 0.184 x 0.020	0.256 x 0.097 x 0.033
ϑ-range for data collect (°)	2.973 to 28.842	3.081 to 29.011
Index ranges	-6≤h≤7, -14≤k≤14, -14≤l≤14	-19≤h≤30, -7≤k≤4, -25≤l≤27
Reflections collected	8440	5382
Independentreflections	2685 [R(int) = 0.0369]	2652 [R(int) = 0.0285]
Observed reflections [I>2σ(	2267	2098
Completeness (%)	99.9 (to ϑ = 25.242°)	99.8 (to ϑ = 25.242°)
Refinement method	Full-matrix least-squares on F	Full-matrix least-squares on F
Data / restraints / paramete	2685 / 67 / 207	2652 / 49 / 206
Goodness-of-fit on F^2	1.080	1.073
Final R indices[a] [I>2σ(I)]	R1 = 0.0357, wR2 = 0.0691	R1 = 0.0385, wR2 = 0.0780
R indices (all data)	R1 = 0.0469, wR2 = 0.0732	R1 = 0.0542, wR2 = 0.0845
Larg. diff. peak &hole (e.Å^{-3}	0.264 and −0.316 e.Å^{-3}	0.274 and -0.284

[a] $R_1=\Sigma||F_o|-|F_c||/\Sigma|F_o|$, $wR_2=[\Sigma w(|F_o|^2-|F_c|^2)^2/\Sigma w(|F_o|^2)^2]^{1/2}$

Regarding the structural study performed on solid oVaTPNH2,[19] the relative orientation of the S atom in the heterocycle could be compatible with a tridentate behaviour of the ligand, as it has been observed in related compounds.[20-23] However, in both complexes only N and O atoms are involved in coordination. Results of calculations in the gas phase and of those taking into account solvent effects (not shown) indicate that the more stable conformer has the thiophene ring rotated in approximately 90 degrees from the benzene ring plane, a conformation that prevents the S atom from coordination. In Figure 2, shows the crystal packing of both complexes, it can be appreciated that the rotation angle of the thiophene ring is almost coincident with the one predicted in the gas phase. Thus, the lattice

stabilization effect due to coordination to the metal is probably not strong enough to compensate for the conformational change needed by the ligand to act as tridentate.
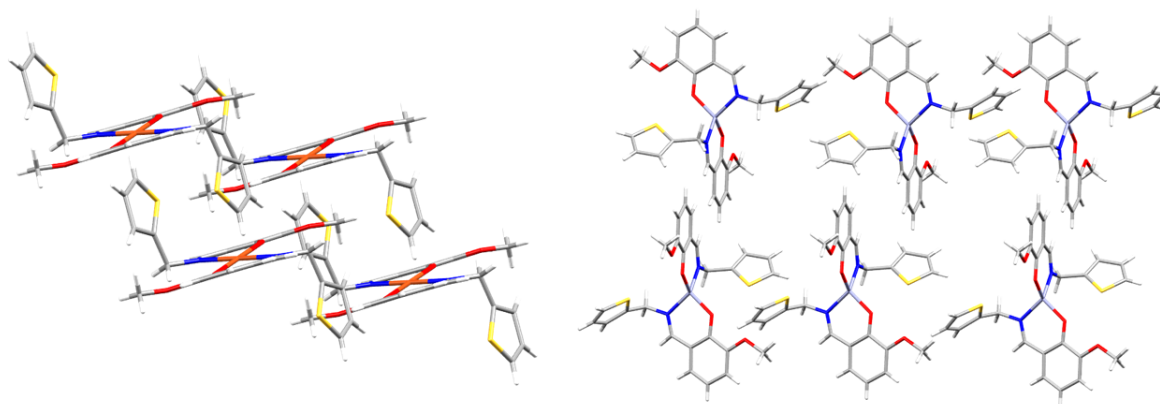
Figure 2. Crystal packing of CuL$_2$ (left) and ZnL (right)

3.2. Optimized geometries and their comparison with experimental data Deleted section

Geometrical parameters of both complexes were optimized using the computational procedure described in the experimental section 4.4 (see below). Geometrical parameters are listed in Table S6 of the Supplementary Information where the results for CuL$_2$ and ZnL$_2$ are compared with the experimental crystallographic data.

Optimized geometrical parameters for CuL$_2$ show that the two ligands surrounding the metal ion are inequivalent, thus giving two values for each geometrical parameter. For bond distances and bond angles, the difference among the two calculated values for each inequivalent ligand is small, and therefore only average values are listed in Table S6. Nevertheless, as significant differences are observed in calculated dihedral angles of the two ligands, both values are included in the table. On the other hand, both ligands in complex ZnL$_2$ are equivalent according to present calculations.

It can be appreciated in Table S6 that bond distances around metal ions are well described by the computational methodology used in this work. Calculated N-M bond distance is overestimated by 0.024 and 0.030 Å for CuL$_2$ and ZnL$_2$, respectively. For the O-M bond distance, calculated values also overestimated experimental data by 0.047 and 0.024 Å for CuL$_2$ and ZnL$_2$, respectively. Bond angles are very well described for Zn(II) complex with a maximum error of about 4 degrees. On the other hand, the bond angles with larger errors are those angles involved in the closest environment of Cu(II) ion. Errors are as large as 20 degrees for N-Cu-N' and O1-Cu-O1'.

Dihedral angles are also well described by the computational methodology used in the present work. Not surprisingly, the larger deviations from experimental data are observed in those angles involving the Cu(II) ion in the complex. C5'-N'-Cu-O1, C8-O1-Cu-N', C8'-O1'-Cu-N and C6'-N'-Cu-O1 dihedral angles show errors in a range from 20 to almost 40 degrees. Although C1-C5-N-C6 and C1-C5-N-Zn

~~angles depart from experimental values by about 40 degrees, the environment around the Zn(II) ion is well described. Interestingly, the S-C1-C5-N angles exhibit the largest deviation from experimental measurements in both complexes~~

3.2. Vibrational Spectroscopy

FTIR and Raman spectra of the complexes were registered and are presented in Figure S1 as Supplementary Information, they were analysed in comparison with the spectra of the free ligand we have previously reported. [19] Assignments were done based on reported data [43,44] and results on related species [13,45], and also assisted by DFT calculations. Changes in the frequency of the ligand vibrational modes were observed upon coordination to the metal. Moreover, new bands due to ligand-metal bonds appeared in the spectra of the complexes. The more relevant spectral region in the IR spectra of the ligand and the complexes is depicted in Figure 3. Selected relevant bands, assigned to modes involving coordinating atoms, are listed in Table 2 and a more complete list of spectroscopic information is available as supplementary information (table S6). As can be seen in the tables, calculations predicted a strong coupling of different modes at some frequencies.
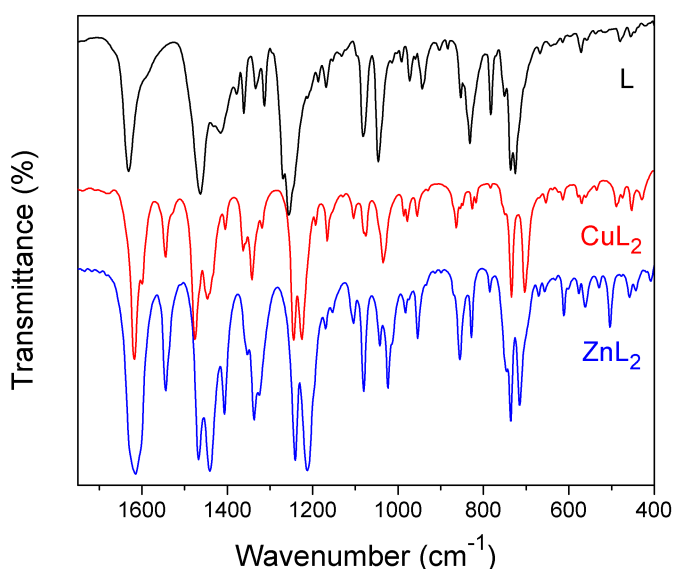
Figure 3. IR spectra of the oVATPNH2 ligand (L) and the complexes CuL_2 and ZnL_2

As predicted, upon deprotonation of the phenolic group, the bands related to the O-H vibrations of the free ligand are absent in the spectra of the complexes. The strong C=N stretching band at 1631 cm^{-1} (IR) and 1635 cm^{-1} (Ra) in the ligand is shifted to lower wavenumbers in the complexes as the N atom participates in the coordination to the metal. As expected, weak bands assigned to the metal-ligand symmetric and anti-symmetric stretching are observed in the lower frequency region of the complexes'

spectra. In both cases, the O-M-O bands appear at higher wavenumbers than the N-M-N ones, as predicted by calculations and in accordance with the M-N distances longer than the M-O ones, also observed in related complexes involving N,O-donor ligands. The –N=C-C-C-O- moiety of each ligand bonded to the metal ion gives rise to a six-membered ring (coordination ring). In the complexes, vibrations of these rings are predicted at lower frequencies that the respective modes of the oVA ring. The ring stretching bands could not be detected, probably because they are overlapped with the intense bands near 1500 cm^{-1}, due to the CH$_3$ and CH$_2$ bending modes. Nevertheless, weak bands related to de coordination ring deformations appeared at around 600 cm^{-1} (in-plane) and 400 cm^{-1} (out-of-plane).

Modes related to the o-Va and thiophene ring vibrations and those concerning the –CH$_2$ and O-CH$_3$ groups show slight changes in frequency and/or intensity upon complex formation, as they are not directly affected by coordination. In particular for CuL$_2$ two close, or even coincident, values are calculated for each mode of the ligand in the complex. This is due to the presence of two no strictly equivalent ligands in the coordination sphere of the metal centre.

Table 2. Relevant bands in the vibrational spectra of CuL$_2$ and ZnL$_2$. Assignment and comparison with the free ligand data (wavenumbers in cm^{-1})

oVATPNH2 (a)				Cu(oVATPNH2)$_2$				Zn(oVATPNH2)$_2$			
IR.	Raman	Calc	Assignment	IR	Raman	Calc.	Assignment	IR	Raman	Calc	Assignment
3003 vw	3005 w	3153	ν O-H								
1631 vs	1635 vs	1685	ν C=N	1618 vs	1624 s	1665/1659	ν C=N	1615 vs	1628 s	1660/1651	ν C=N
1583 sh	1587 m	1660	ν ring (oVA)	1599 m	1602 sh					1642	
		1618	+ δ O-H	1545 m	1546 m	1640/1639	ν ring (oVA)	1544 m	1546 m	1640	ν ring (oVA)
1415 m,b		1480	δ CH$_2$	1405 w	1404 sh	1489/1484	δ CH$_2$	1407 m	1420 sh	1491/1474	δ CH$_2$ + δ$_s$ CH$_3$
		1460	δ O-H + δ$_s$ CH$_3$			1472	ν coord. ring +δ CH$_2$ + δ$_s$ CH$_3$			1465/1461	ν coord. ring + δ CH$_2$ + δ$_s$ CH$_3$
			+ δ C-H(oVA)								
1361 m	1365 w	1370	δ O-H + ν ring (oHVA)	1363 m	1373 m	1462/1464	ν ring (oVA + Tph)+δ$_s$ CH$_2$	1353 w, b	1360 s	1393/1394	ν ring (oVA + Tph) + δ CH (ArCH) + ρ$_w$ CH$_2$
					1370 sh	1440/1433	δ C-H (Ar-CH)				
832 ms,b	838 w	851	γ O-H								
				489 vw	471 w	565	ν$_{as}$ O-Cu-O	477 vvw		568	ν$_{as}$ O-Zn-O
				475 vw		559	ν$_s$ O-Cu-O			563	ν$_s$ O-Zn-O
				453 vw	454 sh	420	ν$_{as}$ N-Cu-N	458 vw	461 vw	461	ν$_{as}$ N-Zn-N
				429 vw		401	ν$_s$ N-Cu-N	443 vw	441 sh	455	ν$_s$ N-Zn-N
					408 vw	370	γ coord. ring	408 vw		411	γ coord. ring

(a) Data extracted from ref [19]. vs: very strong, s: strong, m: medium, w: weak, vw: very weak, b: broad, sh: shoulder: Tph: thiophene ring.

3.3. EPR Spectroscopy.

X-band EPR spectra of powdered solid samples of CuL_2 at different temperatures are given as ESI (Figure S2). No relevant variations are observed in the studied temperature range. Despite the shape of the signal resembles an axial symmetry feature, the best fit is obtained for a rhombic distortion (see Figure 4). The calculated g-values are g_1 = 2.240, g_2 = 2.065 and g_3 = 2.043, where the value of g_1 is calculated with some uncertainty due to the broadness and weakness of the absorption in the parallel component. All the spectra are characteristic of $d_{x^2-y^2}$ ground-state, in good agreement with the square-planar geometry around the metal centre in the crystal.
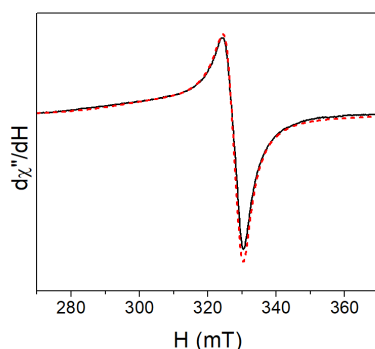
Figure 4. EPR spectrum of $[Cu(oVATPNH2)_2]$ (**CuL₂**) at 150 K (solid line) together with the best fit (dashed line). Experimental details: modulation amplitude 0.1 mT, time constant 40.96 ms, conversion time 327.68 ms, gain 1 10^3 (short ranges) or 1 10^4 (long 0 – 700 mT ranges) and power 20 mW. Microwave frequency 9.4260 GHz.

Calculated G-value [46] is 4.44 (see Equation 1), which suggests negligible magnetic exchange interactions, as expected for the monomeric character of the paramagnetic centre, in agreement with the vibrational spectroscopic results and supporting the predicted structure.

$$G = \frac{g_{\parallel} - 2}{g_{\perp} - 2}$$ Equation 1

In order to have some information about the behaviour of the complex in solution, the X-band EPR spectra of a CuL_2 5 10^{-4} M in (1:1) (DMSO:ethanol) are recorded. The room temperature spectrum is depicted in Figure S3 (ESI). Despite the low resolution, g_{iso} = 2.115 and A_{iso} = 82 G (81.0 10^{-4} cm^{-1}) parameters can be deduced. The measurements carried out in frozen solution at 150 K are characteristic of a $d_{x^2-y^2}$ ground-state (Figure S4), and the best fit yields the following values: $g_{\parallel}$ = 2.224; $A_{\parallel}$ = 185 G (192.1 10^{-4} cm^{-1}); and $g_{\perp}$ = 2.055. The analogies of these g-values with those calculated in solid state suggest that the molecular structure is roughly retained in solution. Finally, the representation of $A_{\parallel}$ vs. $g_{\parallel}$ falls in the area predicted by Blumberg and Peisach Peisach, [47] for Cu(II) complexes with 2N2O planar moieties, in good agreement with the coordination environment in CuL_2.

3.4. Electronic Spectroscopy

Electronic spectra of the complexes are recorded in DMSO solution (approximately 10^{-3} M and 10^{-5} M) in the 250-800 nm spectral range and diffuse reflectance spectra of the solids are also measured (see Figure 5).

Spectra in solution of the ligand and the complexes do not change during 48 hours, hence denoting their stability in the selected solvent. The absorption bands in solution were assigned with the assistance of theoretical calculations. Calculated electronic transitions are selected according to their oscillator strengths. Experimental and calculated spectra for each complex show a good accordance, as can be seen in Figure 5.
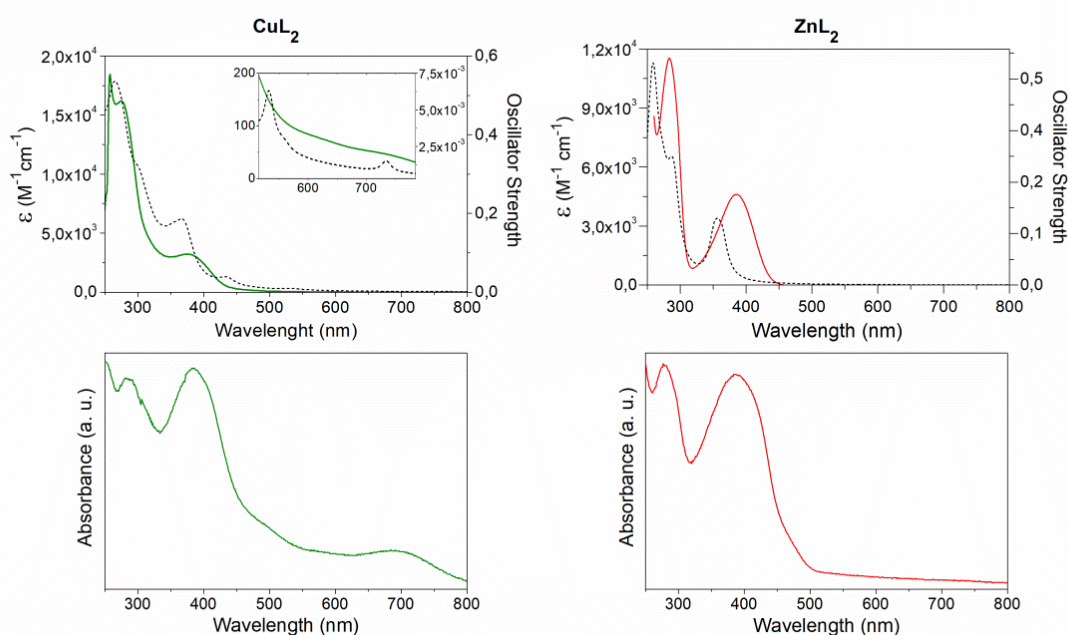
Figure 5: Top: Experimental (solid) and calculated (dashed) electronic spectra of the complexes registered for 5×10^{-5} M DMSO solutions. Higher concentration (5×10^{-3} M) was employed to register *d-d* transitions in complexes CuL$_2$. Bottom: Diffuse reflectance spectra of solid samples.

Table 3 lists experimental bands and calculated electronic transitions for the complexes, along with their assignment. The positions of the maxima are determined by deconvolution of the experimental spectra in the poorly resolved regions. Maxima of the higher energy bands are approximate, due to the proximity of the solvent cut-off. Present calculations show that many-body effects are far from negligible as most of calculated transitions are described by several one-electron excitations, thus involving several MO's. To simplify the description of transitions and the corresponding assignment of experimental bands, an arbitrary threshold to the one-electron excitation coefficients obtained from the TD-DFT is imposed. This way, the number of one-electron excitations selected to describe the

experimental bands is considerably reduced. Graphical representations of the OM's involved in the electronic transitions of CuL_2 and ZnL_2 (Figures S5 and S6, respectively) and their description are available as ESI.

When compared with the electronic spectra ofoVATPNH2, a blue shift of the intra ligand bands (at 263 and 331 nm in the free ligand) is observed in both complexes, as a consequence of coordination. Furthermore, charge transfer bands appear in the spectra in the expected wavelengths. It is interesting to mention that, d-d bands in the Cu(II) complex observed at 693 and 617 nm in solution and at 692 and 587 nm in the solid state are in accordance with a planar square environment of the d^9 copper ion. Even though three bands are predicted for this symmetry, the one at higher energy is frequently hidden under the stronger charge transfer band. [48,49] In this case, deconvolution of the broad band at 381 nm shows the best fit considering two maxima, in accordance with the calculated transition.

The shifts in the band positions and the differences in intensity between the diffuse reflectance spectra obtained from the solid sample and the absorbance spectra in solution of each compound are a consequence of the different physical basis of both measurement method, the way in that data is analyzed and the expected solvent effect. [50] The results indicate that there are no significant changes in the metal environment when compared solid samples with solutions.

Transitions at higher energy are predicted by calculations but they are expected at a lower wavelength than the solvent cut-off. It is worth noting that many experimental bands are described by more than one single electronic calculated transition.

Table 3. Experimental and calculated electronic spectra of the complexes in DMSO solution. Band maxima and transition energies are given in nm. Molar absorptivity (in $M^{-1}.cm^{-1}$) and calculated oscillator strength (in atomic units) are in parentheses. The proposed assignment is also given. H and L are used as short notation for HOMO and LUMO, respectively, whereas α and β refer to the electronic spin channels, when needed.

Experimental	Calculated	Transition	Assignment
CuL$_2$			
693 (51)	735 (0.0007)	$H_\beta \to L_\beta$	$d \to d$
617 (18)	532 (0.0034)	$H_\beta - 10 \to L_\beta$	$d \to d$
558 (35)*	435 (0.0193)	$H_\beta \to L_\beta$	$d \to d$ Ligand-to-metal charge transfer
381 (3.2 x10^3)	370 (0.0588)	$H_\alpha \to L_\alpha +1$ $H_\beta \to L_\beta +2$	Intra- and interligand
289 (sh)	303 (0.0634)	$H_\beta - 3 \to L_\beta +2$	Intraligand
	302 (0.0623)	$H_\beta - 8 \to L_\beta$	Ligand-to-metal charge transfer
276 (1.6 x10^4)	262 (0.1605)	$H_\alpha - 6 \to L_\alpha$ $H_\alpha - 5 \to L_\alpha$ $H_\beta - 4 \to L_\beta + 2$	Intra- and interligand
258 (**)	228 (0.1933)	$H_\alpha - 4 \to L_\alpha +2$	Intra- and interligand
ZnL$_2$			
383 (4.6 x10^3)	363.6 (0.0517)	$H \to L$	Intra- and interligand
283 (9.3 x10^3)	290.1 (0.1505)	$H - 2 \to L$	Intra- and interligand
	273.0 (0.0907)	$H - 8 \to L$	Intra- and interligand Metal-to-ligand charge transfer
259 (**)	258.7 (0.3105)	$H - 5 \to L$	Intra- and interligand

(*) The transition calculated at 435 nm in complex CuL$_2$ presents two monoelectronic components from the HOMO$_\beta$ – 13 and the HOMO$_\beta$ – 23 to the LUMO$_\beta$, which are responsible for the lower wavelength of this transition with respect to the one calculated at 735 nm. The band found at 558 nm by deconvolution is hidden under the strong absorption with maximum at 381 nm.
(**) Undefined maxima due to solvent cut-off.

3.5. NMR Spectroscopy

In order to complete the characterization of the ZnL$_2$ complex in solution, ^{1}H and ^{13}C NMR spectral in $(CD_3)_2SO$ were recorded and compared with those obtained for the free ligand.[19] Table 4 shows the positions and assignments of the signals. As expected, the deprotonation of the OH group in the ligand is evident in the complex. The results are consistent with the proposed coordination feature, as the atoms near the donor set are those with larger variations in the chemical shifts. Figures of the spectra and 2D registers are included in ESI (Figures S7-S10)

Table 4. ^1H and ^{13}C NMR of complex ZnL_2 in $(CD_3)_2SO$ solution. Data for the HL ligand is included for comparison. Chemical shifts δ (ppm), J (Hz) and assignments.

C/H	^1H NMR		^{13}C NMR	
	ZnL_2	HL	ZnL_2	HL
C6	8.44 (s, 1H)	8.68 (s)	171.51	166.78
C8	-	13.35 (s)	161.81	150.83
C9	-	-	152.02	147.90
C1	-	-	139.13	141.31
C3	7.33 (d, J = 5.1 Hz, 1H)	7.03 (dd, J = 5.0, 3.5 Hz)	127.62	127.13
C4	6.92 – 6.72 (m, 4H)	7.47 (dd, J = 5.0, 1.1 Hz)	127.38	125.48
C2	6.92 – 6.72 (m, 4H)	7.06 (m)	127.03	125.45
C12	6.92 – 6.72 (m, 4H)	7.06 (m)	126.47	123.22
C7	-	-	117.59	118.43
C11	6.45 (t, J = 7.8 Hz, 1H)	6.84 (dd, J = 8.3, 7.5 Hz)	115.34	118.18
C10	6.92 – 6.72 (m, 4H)	7.06 (m)	112.55	114.99
C5	4.63 (s, 2H)	4.99 (s)	56.64	56.26
C13	3.65 (s, 3H)	3.78 (s)	55.65	55.74

S:singlet, d: doublet, m: multiplet

3.6. Thermal analysis

The thermal behaviors of the ligand and the complexes were studied analyzing the TG and DT data obtained through the incineration of solid in oxygen flux (see Figure S11 in ESI).

In the TG and DT curves of the ligand, the melting point is observed at 70.5°C. At 165°C starts the decomposition involving several exothermic processes, losing the 59% of mass in a first step, consistent with the removal of the substituted benzene ring fragment. This is followed by the loss of the remaining ligand´s fragments, leading to a total weight loss of 97%.

For the CuL_2 the melting point is observed at 227°C followed by its decomposition which takes place in several steps. The first one, corresponding to a weight loss of 27.0% at 213°C, is consistent with the loss of the (oVA + C=N) fragment (calculated weight loss of 26.8%). The second weight loss (58.0%) occurs with several exothermic processes from 277°C to 717°C, and corresponds to the removal of the remaining ligand, obtaining CuO as residue (corroborated by FTIR spectroscopy, 593, 527 cm^{-1}).

The analysis of the curves of ZnL_2 shows the melting point at 195°C and a decomposition beginning at 239°C with a first loss of 31.0% and a second one of 52.9% at 403°C, consistent with the loss of both ligands. The residue of 15.1% corresponds to ZnO (calculated 14.6%; IR: 482, 448 cm^{-1}).

Due to the thermal inertia during the heating process in the TG experiment, the recorded melting point values of the complexes have some differences with those determined in a Bockmonoscop "M" instrument.

3.7. Cytotoxicity Assays. Evaluation of metal dependent activity on cell viability in breast cancer cell lines (MCF7 and MDA-MB-231).

To test the effect of metal dependent cytotoxicity on cell viability two different breast cancer cell lines: MCF7 (breast adenocarcinoma) and MDA-MB-231 (triple negative breast adenocarcinoma) were assayed. These tumor cells were exposed to the ligand, the metal cation and the complex during 48 h. The anticancer activity of both complexes was investigated and compared with that of the free ligand (oVATPNH2) and respectively with CuII), Zn(II)) ions.

Table 5 shows the IC_{50} values of the complexes and data for the reference metallodrug cisplatin (CDDP) are included for comparison. As it can be seen, both complexes impaired cell viability on MCF7 and MDA-MB-231 cells in the range of concentration (10-50 µM). The table also indicates that CuL_2 is a stronger antiproliferative agent than ZnL_2 and has an even stronger anticancer activity than CDDP in both tested breast cell lines. On the other hand, the IC_{50} values of the free ligand and free metal cations are greater than 100 µM for both cell lines tested, hence revealing the important role of complexation to modulate the antitumor properties of this kind of compounds.

Table 5. IC_{50} (µM) values of complexes and CDDP on MCF7 and MDA-MB-231 after 48 h of incubation. Values for free ligand and metal ions are included for comparison.

Cell line	L	CuL_2	ZnL_2	CDDP	Cu(II)	Zn(II)
MCF7	> 100	13.9 ± 3.3	43.6 ± 0.16	19.3 ± 2.1	> 100	> 100
MDA-MB-231	> 100	23.0 ± 1.52	41.7 ± 2.88	27.5 ± 2.14	> 100	> 100

This positive effect has been described for other complexes of these metals and others such as platinum and palladium that have shown cytotoxic activity. [51,52] Particularly, copper have been more effective against both breast cancer cell lines (MCF7 and MDA-MB-231) than zinc. Comparison of IC_{50} values with other copper complexes reveals that this complex can be included in the active group, as a potential cytotoxic agent. [53] In this sense, copper(II) complex of 4'methoxy-5,7-dihydroxy-isoflavone showed moderate cytotoxic effectiveness against human breast cancer cells with IC_{50} values in the 20-50 µM range. [54] It is also important to highlight that even though copper(II) complexes with mononegative bidentate S,N-Schiff bases derived from S-benzyl- and S-methyl dithiocarbazate showed selective activity against MCF-7 cells (IC_{50}= 0.45 µM), they were inactive against MDA- MB-

231 cells. [55] The same cell specificity was observed for copper complexes with Schiff bases benzyl N-[1-(thiophen-2-yl)ethylidene] hydrazine carbodithioate and benzyl N-[1-(thio- phen-3-yl)ethylidene].[56] The effectiveness of copper complex could be associated with its planar conformation, but further mechanistic studies are required to determine the correlation. Results have been reported on some copper complexes more effective than platinum compounds as antitumor agents on prostate and breast and cancer cells. [57] Considering that generally copper compounds have less toxic side effects than platinum ones [58,59] it would be interesting to test this complex in further in vivo studies for breast cancer treatments.

4. Conclusions

The interaction of oVATPNH2 with Cu(II) and Zn(II) lead to the formation of stable complexes, namely [Cu(oVATPNH2)$_2$] (CuL$_2$) and [Zn(oVATPNH2)$_2$] (ZnL$_2$). Despite the presence of the S, N and O donor atoms in the ligand, it acts as a bidentate ligand through the phenoxo oxygen and the imine nitrogen atoms in both complexes.

The crystal structures of the complexes reveal a nearly square planar environment for the copper centre and a tetrahedral coordination sphere in the case of Zn cation. In both cases the thiophene ring appears almost perpendicular to the coordination plane in the ligand, increasing the deviation from the benzenic ring as compared with the free ligand.

Spectroscopic behaviour completely accords with the structural properties of the complexes and reveals that the coordination sphere is retained in solution. Calculated parameters and frequencies assisted the interpretation of the experimental results and show good agreement. The vibrational modes of the free ligand are consequently changed upon its deprotonation followed by coordination to the metal and new bands related to metal-ligand bonds are observed. For CuL$_2$, the EPR spectra are characteristic of a $d_{x^2-y^2}$ ground-states and the expected *d-d* transitions can be identified in the electronic spectra, according to the distorted square-planar environment of the Cu(II) centre.

Cytotoxicity studies on two breast cancer cell lines show the beneficial effect of metal complexation on the antitumoral action compared with either the free ligand or the metal ions independently. The copper complex is more active against both lines, with IC$_{50}$ values lower than those of CDDP. Considering the lower toxicity of copper with platinum and the limitations in the treatment of triple-negative breast adenocarcinoma, CuL$_2$ could be considered an interesting candidate for the development of new antitumor agents.

Electronic Supplementary Information

Crystallographic structural data have been deposited at the Cambridge Crystallographic Data Centre (CCDC). Enquiries for data can be direct to: Cambridge Crystallographic Data Centre, 12 Union Road, Cambridge, UK, CB2 1EZ or (e-mail) deposit@ccdc.cam.ac.uk or (fax) +44 (0) 1223 336033. Any request to the Cambridge Crystallographic Data Centre for this material should quote the full literature citation and the reference numbers CCDC1844563 for complex CuL_2 and 1844564for complex ZnL_2.

Geometrical parameters for complex CuL_2 and ZnL_2 (Tables S1 to S5); experimental and vibrational spectra along with the assignment (Table S6), FTIR and Raman spectra in the whole spectral range (Figure S1); EPR spectra of CuL_2 solid sample (Figures S2) and in solution (Figures S3 and S4) at different temperatures, MOs involved in relevant electronic transitions of the complexes (Figures S5 and S6) and their description; RMN spectra for ZnL_2 (Figures S7 to S10) and TG and DTA thermograms of both complexes (Figure S11) are available as ESI.

Conflicts of Interest

There are no conflicts of interest to declare.

References

1 - G L. Backes, D. M. Neumann, B. S. Jursic, *Bioorg. Med. Chem*. 2014, **22**,4629-4636.

2 - C. M. da Silva, D. L. da Silva, L. V. Modolo, R. B. Alves, M. A. de Resende, C. V. B. Martins, Â. de Fátima, *J. Adv. Res*. 2011, **2**, 1-8.

3 - S. A. Matar, W. H. Talib, M. S. Mustafa, M. S. Mubarak, M. A. AlDamen, *Arab. J. Chem*. 2015, **8**, 850-857.

4 - M. Rudrapal, B. De, *Int. Res. J. Pure. Appl*. Chem. 2013, **3(3)**, 232-249.

5 - A. B. Gündüzalp, N. Özbek, N. Karacan, *Med. Chem. Res*. 2012, **21**, 3435-3444.

6 - S. Bala, S. Kamboj and A. Kumar, *J. Pharm Res*. 2010, **3(12)**, 2993-2997.

7 - L. N. F. Cardoso, T. C. M. Nogueira, F. A. R. Rodrigues, A. C. Aragão Oliveira, M. C. dos Santos Luciano, C. Pessoa and M. V. N. de Souza, *Med. Chem. Res*. 2017, **26(8)** 1605-1608.

8 - S. Kumar, D.N. Dahr, and P.N. Saxena, *J. Ind. Sci. Res.* 2009, **68**, 181-187.

9 - W. Al Zoubi Int. *J. Org. Chem*. 2013, **3**, 73-95.

10- X. Liu , C. Manzur , N. Novoa, S. Celedón, D. Carrillo and J. R. Hamon, *Coord. Chem. Rev*. 2018, **357**, 144-172.

11 - A. B. Gündüzalp, I. Özsen, H. Alyar, S. Alyar, N. Ozbek, *J. Mol. Struct*. 2016, **1120**, 259-266.

12 - R. Katwal, H. Kaura, B. K. Kapur *Sci. Revs. Chem. Commun*. 2013, **3(1)**, 1-15.

13 - M. Khorshidifard, H. A. Rudbari, Z. Kazemi-Delikani, V. Mirkhani, R. Azadbakht, *J. Mol. Struct.* 2015, **1081**, 494-505.

14 - S. A. da Silva, C. Q. F. Leite, F. R. Pavan, N. Masciocchi, A. Cuin*, Polyhedron*, 2014, **79**, 170-177.

15 - C. Spînu, M. Pleniceanu, C. Tigae, *J. Chem. Serb. Soc.* 2008, **73**, 415-421.

16 - M. Mishra, K. Tiwari, S. Shukla, R. Mishra, V.P. Singh, *Spectrochim. Acta*, 2014, **132**, 452-454.

17 - I. E. León, J. F. Cadavid-Vargas, A. L. Di Virgilio, S. B. Etcheverry, *Curr. Med.Chem*. 2017, **24(2)**, 112-148.

18 - J. A. de la Mare, L. Contu, M. C. Hunter, B. Moyo, J. N. Sterrenberg, K. C. Dhanani, L. Z. Mutsvunguma and A. L. Edkins. *Recent Pat. Anticancer Drug Discov*. 2014, **9(2)**, 153-175.

19 - M. R. Rodríguez, J. Del Plá, O. E. Piro, G. A. Echeverría, G. Espino, R. Pis-Diez, B. S. Parajón-Costa, A C. González-Baró, *J. Mol. Struct*. 2018, **1165**, 381-390.

20 - M. N. Patel, C. R. Patel, H. N. Joshi, *Z. Anorg. Allg. Chem.* 2012, **638, (7-8)**, 1224-1232.

21- C. Spinu, A. Kriza, *Acta Chim. Slov.* 2000, **47**, 179-185

22 - A. B. Gündüzalp, B. Erk, *Russian Journal of Inorganic Chemistry,* 2010, **55(7)**, 1094-1102.

23 - J. F. Modder, J-M. Ernsting, K. Vrieze, M. de Wit, C.r H. Siam, G. van Koten1, *Inorg. Chem.* 1991, **30**, 1208-1214.

24 - CrysAlisPro, Oxford Diffraction Ltd., version 1.171.33.48 (release 15-09-2009 CrysAlis171.NET)

25 - G. M. Sheldrick, *Acta Crystallogr*. 2008, **A64**, 112-122.

26 - SimFonia v1.25, Bruker Analytische Messtecnik GmßH, 1996.

27 - Kaleidagraph v3.5 Synergy Software, 2000.

28 - G. R. Fulmer, A. J. M. Miller, N. H. Sherden, H. E. Gottlieb, A. Nudelman, B. M. Stoltz, J. E. Bercaw, K. I. Goldberg, *Organometallics* 2010, **29**, 2176-217.

29 - D. Becke, *J. Chem. Phys*. 1993, **98**, 5648-5652.

30 - C. Lee, W. Yang, R. G. Parr, *Phys. Rev.* 1988, **B 37**, 785-789.

31 - F. Neese, Wiley *Interdiscip. Rev. Comput. Mol. Sci*. 2012, **2**, 73-78.

32 - F. Weigend, R. Ahlrichs, *Phys. Chem. Chem. Phys*. 2005, **7**, 3297-3305.

33 - C. Adamo, V. Barone, *J. Chem. Phys*. 1999, **110**, 6158-6170.

34 - A. Klamt, G. Schüürmann, *J. Chem. Soc., Perkin Trans.* 1993, **2**, 799-805.

35 - T.T. Mosmann, *J. Immunol. Methods*, 1983, **65**, 55-63.

36 - L. J. Farrugia, *J. Appl. Cryst.* 1997, **30**, 565.

37 - N. Novoa, T. Roisnel, P. Hamon, S. Kahlal, C. Manzur, H. M. Ngo, I. Ledoux-Rak, J. Y. Saillard, D. Carrillo, J. R. Hamon, *Dalton. Trans.* 2015, **44**, 18019-18037.

38 – N. Revathi, M. Sankarganesh, J. Rajesh, J. D. Raja, *J. Fluoresc.* 2017, **27**, 1801-1814.

39 - S. Sangeeta, K. Ahmad, N. Noorussabah, S. Bharti, M. K. Mishra, S. R. Sharma, M. Choudhary, *J. Mol. Struct.* 2018, **1156**, 1-11.

40 – M. Enamullah, G. Makhloufi, R. Ahmed, B. A. Joy, M. A. Islam, D. Padula, H Hunter, G. Pescitelli, C. Janiak, *Inorg. Chem.* 2016, **55**, 6449-6464.

41 – M. Khorshidifard, H. A. Rudbari, B. Askari, M. Sahihi, M. R. Farsani, F. Jalilian, G. Bruno, *Polyhedron*, 2015, **95**, 1-13.

42 - M. Montazerozohori, A. Masoudiasl, S. Joohari, J. M. White, *Mater. Sci. Eng*. C, 2017, **77**, 229-244.

43 - D. Lin-Vien, N. B. Colthup, W. G. Fately and J. G. Grasselli in: *Infrared and Raman Characteristic Frequencies of Organic Molecules*, Academic Press, Boston, 1999.

44 - K. Nakamoto, in: *Infrared and Raman Spectra of Inorganic and Coordination Compounds*, Sixth ed., J. Wiley & Sons, Inc., Hoboken, New Jersey, 2009.

45 - A. C. González-Baró, R. Pis-Diez, C. A. Franca, M. H. Torre, B. S. Parajón-Costa, *Polyhedron,* 2010, **29**, 959-968.

46 - B. J Hathaway, D. E. Billing, *Coord. Chem. Rev*. 1970, **5**, 143-207.

47 - J.; Blumberg, W. E. *Arch. Biochem. Biophys.* 1974, **165**, 691–708.

48 - I. M. Procter, B. J. Hathaway, P. Nicholls *J. Chem. Soc. A*, 1968, 1678-1684.

49 - A. B. P. Lever in *Inorganic electronic Spectrocopy*, 2nd Ed. Elsevier, Amsterdam, 1984.

50 - G. Kortüm in *Reflectance Spectroscopy. Principles, Methods, Applications*. Springer-Verlag, New York Inc. 1969.

51 - A. Matesanz , E. Jimenez-Faraco, M. C. Ruiz, L. M. Balsa, C. Navarro-Ranninger, I. E. León, A. G. Quiroga, *Inorg. Chem. Front*. 2018, **5**, 73-83.

52 - I. E. Leon, J. Cadavid-Vargas, I.Tiscornia, V.Porro, S. Castelli, P. Katkar, A. Desideri, M. Bollati-Fogolin, S. Etcheverry *J. Biol. Inorg. Chem*. 2015, **20(7)**, 1175-1191.

53 - Sant- C. ini, M. Pellei, V. Gandin, M. Porchia, F. Tisato, C. Marzano, *Chem. Rev.* 2014, 114, 815-862.

54 - X. Chen, L. J. Tang, Y. N. Sun, P. H. Qiu, G. Liang, *J. Inorg. Biochem*. 2010, **104,** 379-384.

55 - M. A. F. Abdul Manan, M. I. M. Tahir, K. A. Crouse, R. Rosli, F. N. F. How, D. J. Watkin, *J. Chem. Crystallogr*. 2011, **41**, 1866-1871.

56 - M. H. E. Chan, K. A. Crouse, M. I. M. Tahir, R. Rosli, N. Umar-Tsafe, A. R. Cowley, *Polyhedron* 2008, **27**, 1141-1146.

57 - J. Grau, C. Renau, A. B. Caballero, A. Caubet, M. Pockaj, J. Lorenzo and P. *Gamez, Dalton Trans.* 2018, **47(14),** 4902-4908.

58 - T. Wang, Z. Guo, Curr. *Med. Chem.* 2006, **13**, 525-537 and references therein.

59 - C. Marzano, M. Pellei, F. Tisato, C. Santini, *Anti-Cancer Agents Med. Chem*. 2009, **9**, 185-211.